ELSEVIER

Nuclear Physics A 612 (1997) 53–81

NUCLEAR PHYSICS A

The measurement of the beta asymmetry in the decay of polarized neutrons

P. Liaud [a,b,1], K. Schreckenbach [a,2], R. Kossakowski [b], H. Nastoll [a], A. Bussière [b], J.P. Guillaud [b], L. Beck [a,2]

[a] *Institut Laue–Langevin, BP 156X, 38042 Grenoble, France*
[b] *LAPP Annecy, BP 110, 74941 Annecy le Vieux Cédex, France*

Received 17 May 1995; revised 27 August 1996

Abstract

The beta-decay asymmetry parameter A was measured for the free neutron with high precision. A time projection chamber (TPC) and plastic scintillators were used as a track and energy detector for the decay electrons. Thus the decay volume was well defined. Electron tracks with different angle θ between the electron momentum and the neutron spin could be selected and compared with the expected cos θ distribution. A deviation from this distribution was observed and remains unexplained. Using the electron track detector only to delimit the fiducial volume and adopting the theoretically predicted cos θ distribution a value of $A_0 = -0.1160 \pm 0.0015$ was determined including corrections for recoil and weak magnetism. To our best knowledge this result is not influenced by the observed deviation from the cos θ distribution of the asymmetry. From this result the ratio $g_A/g_V = -1.266 \pm 0.004$ can be deduced within the Standard Model. Using the recent neutron lifetime value leads to $g_V = 1.4172\ (34) \cdot 10^{-62}$ J m^3. This value is in good agreement with g_V from $ft(0^+ \rightarrow 0^+)$ and μ decay.

Keywords: RADIOACTIVITY ^{1}n; Beta asymmetry measurement with an helium-filled TPC; Cold polarized neutrons; Standard model

1. Introduction

The measurement of the beta asymmetry and the halflife of the free neutron decay yield the determination of the weak interaction coupling constants g_A and g_V from the neutron decay alone [1]. The coupling constant g_V is a fundamental parameter of the

[1] Present address: Institut des Sciences Nucléaires, 38026 Grenoble, France
[2] Present address: Technische Universität München, Physik Dept. E21, D-85747 Garching, Germany.

PII S0375-9474(96)00325-9

Standard Model. The comparison of g_V measured in $0^+ \rightarrow 0^+$ super allowed beta decay, where the nuclear force is acting, with the g_V value measured in neutron decay, tests the conserved vector current theory (CVC) [1]. The relation between g_V and the Fermi constant G_F, which is best determined in muon decay, defines the Cabibbo angle or more generally the first element of the Cabibbo–Kobayashi–Maskawa (CKM) matrix. The CKM matrix which describes the rotation of the weak interaction quark eigenstates relative to their mass eigenstates should be unitary. With the current values of the matrix elements an independent value of g_V can be obtained using only higher generation decay. Unitary of the quark mixture matrix as well as CVC theory can be tested and verified [1].

Axial vector current non-conservation would allow g_A to change inside nuclei, so free neutron decay is essential for determining g_A. The axial current is not conserved and g_A for nucleons and quarks are different because the quarks interact. Understanding of how this renormalization evolves is an important problem in quantum chromodynamics.

The knowledge of g_V and g_A has an important implication also in astrophysics. As an example the sun energy producing mechanism is dominated by the process $p + p \rightarrow d + e^+ + \nu_e$; this reaction cross section is proportional to g_A^2, but too small to be measured directly in the laboratory. The central temperature of the sun depends on g_A and so do the rates of the other nuclear reactions that take place in the sun as those producing energetic neutrinos.

For a left–right symmetry of grand unification interactions all left-handed particles should have heavy right-handed partners. The mass difference is due to the spontaneous symmetry breaking at higher energy scale. In such models the physical gauge bosons are linear combinations with some mixing angle ε of the right- and left-handed bosons, respectively. Under the symmetry breakdown the squared mass ratio δ of the physical bosons acquires a small value. τ_n, A and the ft value of $0^+ \rightarrow 0^+$ super allowed transitions depend on the weak coupling constants g_A, g_V and on the δ and ε parameters. At low energy small right-handed admixture could be detected [2].

The purpose of the present experiment was the measurement of the asymmetry coefficient A. It is related to the angular distribution of the emission of the beta particle by

$$W(E, \theta) = W_0(E)\left(1 + \frac{v}{c} A \cos \theta\right), \tag{1}$$

$W_0(E)$ is the allowed shape of the beta spectrum of the neutron, v/c the electron velocity relative to the speed of light and θ the angle between the spin of the neutron and the momentum of the electron. In general an asymmetry function is measured in the experiments:

$$\frac{W_\uparrow - W_\downarrow}{W\uparrow + W\downarrow} = \frac{v}{c} A \cos \theta. \tag{2}$$

The signs $\uparrow$ and $\downarrow$ denote the spectrum for two opposite spin directions of the neutron. In general the asymmetry function is measured with the same detector inverting the

direction of the neutron spin by a spin-flip device. For this case Eq. (2) must be corrected for the spin-flip efficiency and degree of polarization in the experiment. Also the detector response function must be taken into account. The measured value of A is slightly different from the asymmetry coefficient A_0 due to recoil and weak magnetism. Including this correction and using the standard V–A theory the ratio of the weak interaction coupling constants $\lambda = g_A/g_V$ can be deduced from this coefficient A_0.

Including the recent measurement of A at the PNPI by Erosolimskii et al. [3] the evaluation of g_V from the neutron decay resulted in a disagreement to g_V from μ decay and $ft(0^+ \rightarrow 0^+)$ at a level of almost three standard deviations. On the other hand, the A_0 value in Ref. [3] of $-0.1116(14)$ agrees within the experimental uncertainty with the other high precise value of Ref. [4] citing $A_0 = -0.1146(19)$. In Ref. [3] the decay electrons were detected within a small angle and in coincidence with a proton detector. Ref. [4] used a superconducting solenoid (''PERKEO'') for guiding the electrons to the plastic scintillator detectors. Thus the asymmetry averaged over cos θ in one half space was determined after some corrections due to magnetic mirror effects for the electrons. Only one detector combined with a neutron spin-flip device was used in these experiments.

In the present experiment the track of the decay electron was measured by an in-beam time projection chamber (TPC) and the energy was determined in plastic scintillators working in coincidence with the TPC. The scintillators were placed in and opposite to the neutron spin direction providing together with a neutron spin-flip device a very symmetric experimental set-up. With this novel method the present work should examine whether the discrepancy in g_V values is real. A first result of the present work was published in Ref. [5].

2. Experimental set-up

The experiment was carried out at the PN7 cold neutron beam position of the ILL High Flux Reactor, Grenoble. A schematic view of the experimental set-up is shown in Fig. 1. The polarizer was placed at 5 m from the detector in a well shielded, separate casemate. The detector and the associated electronics were set-up in a climatized experimental room. In the following the components of the experiment are described.

2.1. The beam-line of polarized neutrons

The unpolarized neutrons come from the ILL H14 neutron guide which views the cold source of the reactor. They have a broad wavelength distribution with a peak flux around 5 Å. The flux at the exit of this guide is 10^9 n cm^{-2}s^{-1}. The neutron beam was limited in size by a 15×25 mm^2 diaphragm (B_4C) at the exit of the H14 guide. The polarizer, mounted on a turnable table, consisted of bent super mirrors [6]. The super mirror device was made of 1 mm spaced glass plates covered on one side by multilayers of Co–Ti on top of an antireflecting GdTi layer. The glass plates were bent over their 35 cm length to prevent a passage of neutrons without any reflection. Permanent magnets

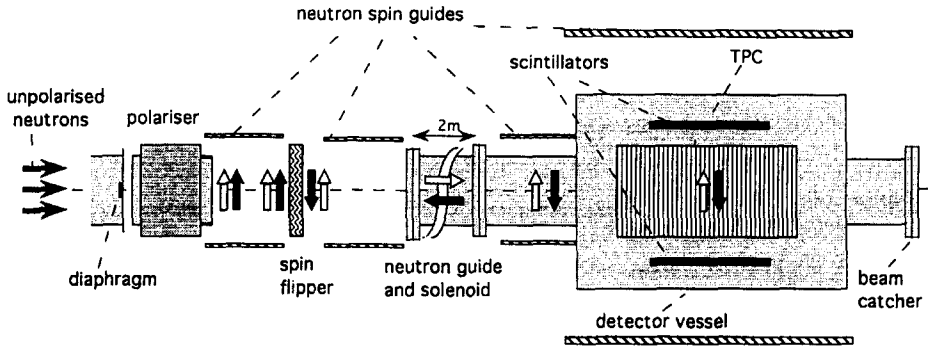

Fig. 1. Schematic view of the experimental set-up. Unpolarized cold neutrons from the ILL cold source were transversaly polarised by a system of bent supermirrors. Further down, the polarized neutrons passed a spin flipper of current sheet type. An adiabatic transformation turns the neutron spin along the neutron beam direction before entering a 2 m long neutron guide placed inside a longitudinal magnetic field of 1 mT. Finally, the polarized neutrons entered the detector vessel which was placed in a transverse 1.2 mT magnetic field. A beam catcher stopped all the neutrons at the exit of the detector vessel. The neutron spin directions are shown through the beam line for spin flipper off and on, respectively. The spin is aligned to the magnetic fields.

magnetized the mirror parallel to its surface, i.e. perpendicular to the beam direction, yielding transversely polarized neutrons. The spin of the transversely polarized neutrons was guided by a weak magnetic field (1 mT) through the beam line. The spin flipper was of the current sheet type [6].

Next in the beam line the neutrons entered a 2 m long neutron guide with uncovered glass walls and an inner cross section of 15×25 mm^2. It was embedded in LiF loaded Epoxy to absorb neutrons not guided. Together with the diaphragm at the H14 neutron guide exit it collimated the neutron beam due to the angle of total reflection at the glass walls. Furthermore it increased the distance from the detector to the polarizer which is an intense source of γ-rays.

The neutron glass guide was placed in the center of a solenoid which created a longitudinal magnetic field of about 1 mT along the guide. The transition from the transverse to the longitudinal field regions was made such that the neutron spin followed adiabatically the magnetic field direction (adiabaticity is fulfilled when the rotation frequency of the magnetic field direction, viewed in the frame of the moving neutrons, is small compared to their Larmor frequency).

The polarized neutron beam passed the TPC with a flux of about 10^8 n/s and a divergency which widened the beam to a maximum size of 3×4 cm^2. The detector vessel was entirely placed in a transverse magnetic field of 1.2 mT. This field was built by two parallel soft iron plates with six soft iron core solenoids across. The currents in the coils could be adjusted such that the magnetic field direction was perpendicular to the detector axis. By a careful tuning the deviation from the perpendicular direction was less than 0.8°. It was determined by a measurement with a Förster sonde of the residual longitudinal field component, which was less than 16 μT [7,8]. The neutrons were finally absorbed in a distant ^{6}LiF beam catcher.

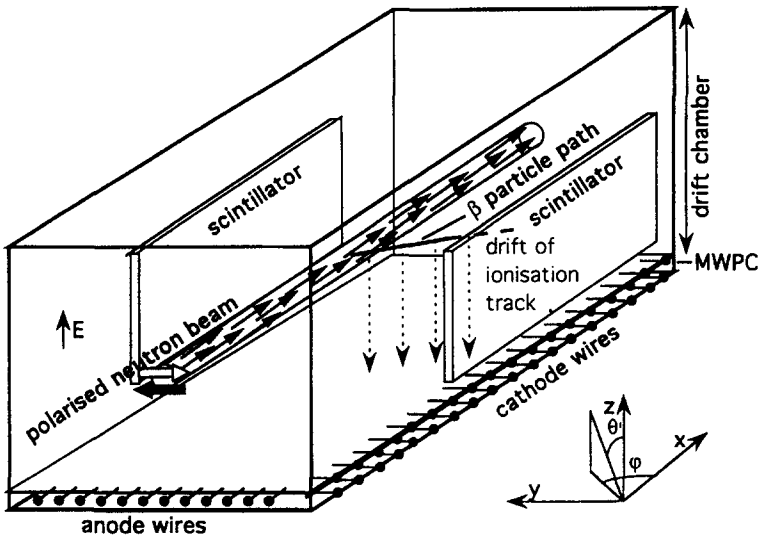

Fig. 2. Drift chamber with two plastic scintillators. The ionisation paths due to the decay electrons are drifted towards the multiwire proportional region (MWPC) under an electrical field E. The anodes and cathodes record respectively the y and x coordinates of the electron path. The third coordinate (z) is obtained via the measurement of the drift time between the signal of the scintillator and the touched anode wires. The black and bold arrow at the entry of the detector represents respectively the neutron spin and the 1.2 mT magnetic field direction in an antiparallel configuration.

2.2. The detector

The detector consisted of a drift time chamber working in a Time Projection Mode, Fig. 2. This TPC was already used in a free neutron lifetime measurement and is described in detail in [9]. For the beta asymmetry measurement two plastic scintillators of 43 cm × 16 cm × 0.5 cm have been added on each side of the TPC. The thickness of 5 mm is sufficient to stop completely the electrons from the neutron decay (beta endpoint energy 782 keV). The scintillator plates were coupled on both ends by light guides to photomultipliers. Calibration sources could be moved in the drift volume along the detector axis by a manipulator.

Fig. 3 shows the response of the scintillator to monoenergetic electrons from conversion lines of ^{207}Bi (K-lines: 973.2 keV and 481.7 keV), ^{113}Sn (363.8 keV) and ^{139}Ce (127.0 keV), measured in coincidence with the TPC without selection of cathode coordinates. The parametrization of the measured line shapes is described in Section 4.3.

The ionisation paths created by the decay electrons were drifted towards the multiwire proportional region (MWPC) by a 175 V/cm drift field. The MWPC consisted of 18 sensitive anode wires (spaced of 1 cm and separated by field wires) and of 20 cathode sections of 2.5 cm width which, respectively, record the y and x coordinates of the path of the beta particle. The third coordinate (z) of the beta trajectory was obtained from the measurement of the drift time, i.e. the time difference between the signal of the plastic scintillator and of the touched anode wires. The

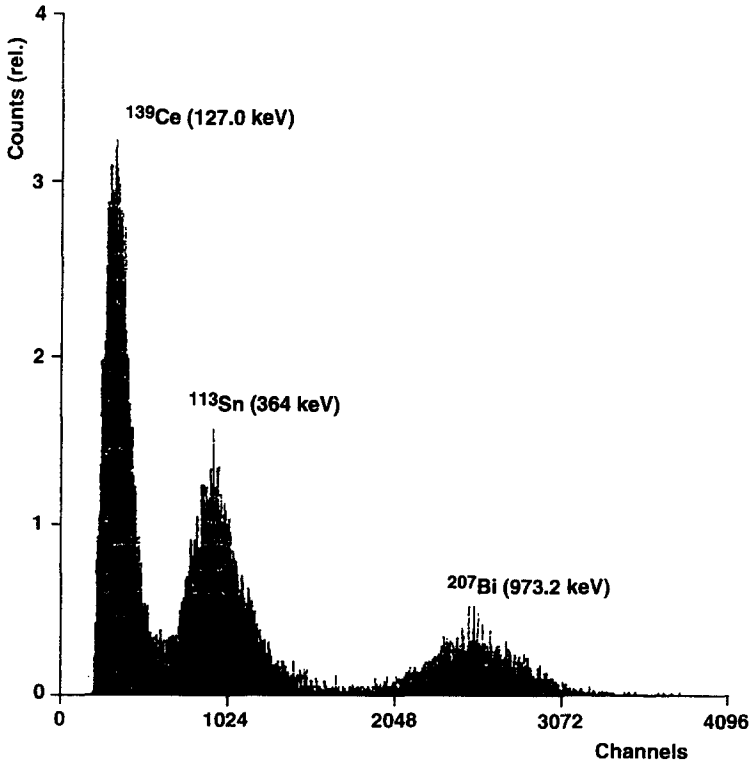

Fig. 3. Response of the plastic scintillator (in coincidence with the TPC) to monoenergetic electrons from conversion lines of ^{139}Ce, ^{113}Sn and ^{207}Bi.

efficiency of detection was greater than 95% for each individual wire. It was determined by the completeness of registered electron tracks from a ^{204}Tl source.

The gas mixture (^{4}He(93%)–CO_2(7%)) was chosen owing to its low capture cross section for slow neutrons (in particular $\sigma_{^4\mathrm{He}} = 0$) as well as for its weak multiple scattering of β particles [10].

2.3. The electronics

Signals from the detector anodes and cathodes were analysed in the timing electronics to determine the time relative to the scintillator signal and the space coordinates of the β particle. For each anode wire the collected charge was converted to a voltage signal by a charge sensitive preamplifier. Time information was obtained from the amplified pulse signal using standard level discriminators. Anode and cathode signals were processed in the same way through similar electronics. The projection of the electron track (xy horizontal plane) is known from the anode and cathode signals fired, which determine these coordinates with a spatial resolution of 1 cm and 2.5 cm, respectively, owing to the wire spacing or grouping. The vertical coordinate (z) is given by the drift velocity being of the order of 0.7 cm/μs. The z resolution was affected by the pulse height

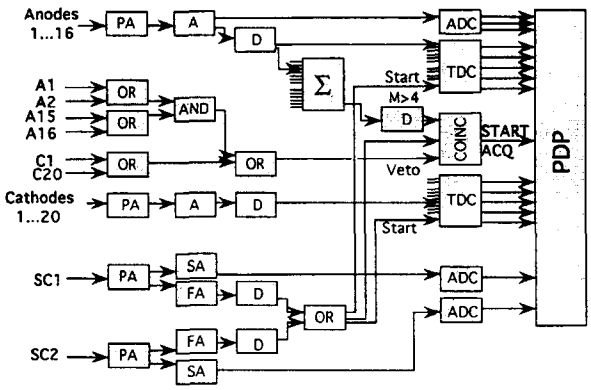

Fig. 4. Simplified electronic scheme. For each anode (A_1 to A_{16}) or cathode (C_1 to C_{20}) the collected charge was converted into a voltage signal by a charge sensitive preamplifier (PA). A veto signal from the extreme cathodes (C_1 and C_{20}) and from both the outermost pairs of anode wires (A_1–A_2 and A_{15}–A_{16}) prevented the recording of signal from particles which pass the whole detector. Σ indicates the summation of the amplitude of the anode signals; only signals for particles which touch at least four anode wires ($M > 4$ on figure) and one of the scintillators (SC_1 or SC_2) were recorded. SA and FA stand respectively for spectroscopy amplifier and fast amplifier; D denotes standard discriminators.

dependence of the time trigger since simple level discriminators were used. With a rise time of the pulses of about 1 μs and a drift velocity in the TPC of 0.7 cm/μs the z resolution was broadened by less than 0.7 cm, which was narrower than the beam size or the x, y resolution. Special time to digital converters (TDC) were built and adjusted for this experiment. The light from the scintillators was collected at both ends of each scintillator by R878 HA Hamamatsu photomultipliers. The amplification of the two photomultiplier signals were tuned such that the pulse heights became equal for a calibration source in the center of the chamber. For a given beta energy, the sum of the signals were then almost independent of the position of the source along the detector axis.

Fig. 4 shows a simplified scheme of the main features of the electronics. An event is recorded if the anode signal corresponds at least to four touched wires ($M \geqslant 4$ in Fig. 4) and one of the scintillators gives a signal in coincidence with the anodes.

By veto signals from cathodes 1, 2, 19 and 20, ionization tracks were rejected which passed the back or front end of the TPC. Thus the effective length of the detection volume was limited to 40 cm. A further veto signal from both the outermost pairs of anode wires (1 or 2) and (17 or 18) prevented the recording of signals from particles which crossed the whole detector; a true event must come from the central part of the TPC where the neutron beam passes. After a signal from the photomultiplier an inhibit signal of 40 μs prevented a possible further signal from interfering.

The spin flipper power supply was driven by a clock and the spin direction stored in a pattern unit; the spin direction relative to the magnetic field was reversed every 5 seconds.

2.4. The data acquisition system

The acquisition of the data was performed by a PDP 11/23 computer. The electronic–computer interface was controlled by standard CAMAC logic. Typically the collected event rate was about 100/second; the acquisition dead time was 2 μs/event.

For each event, containing 64 words of 32 bits, the following information was encoded:

- the scintillator pulse height from the individual PM's;
- the sum of the two PM signals on-line;
- the number and drift time for each anode and cathode wire fired;
- the neutron spin direction.

In order to control the stability of the acquisition conditions a 10 Hz electronic clock produced flagged events in parallel to the physical trigger.

We used a TSX11 system which gave a speedy access to external interruption. The data were written on Exabyte owing to the large amount of data to be collected. The performance of this system allowed us to collect events at a 200 Hz rate without high losses. The 1.5 Gigabyte tape lasted about 20 hours and was evaluated off-line at a VAX computer.

3. Measurements

3.1. Degree of polarization

Fig. 5 displays a scheme of the arrangement used in the beta asymmetry experiment to measure the degree of polarization of the neutron beam (Refs. [7,8]). The unpolarized beam passes a polarizer P_1 of polarizing power p_1 two spin flippers S_1 and S_2 with spin-flip efficiencies s_1 and s_2, and an analyser P_2 with analysing power p_2. Both polarizer and analyser were often supposed to have the same polarizing efficiency ($p_1 = p_2$). Actually p_1 and p_2 are not quite identical, they differ by a small amount even if they are fabricated under similar conditions.

It was shown [7,8] that for a high level of accuracy the permutation of at least three different pairs of polarizer/analyser is essential for the determination of p_1 and p_2 as well as for a reliable determination of the degree of polarization.

For the determination of the values of p_1 and the spin-flip efficiency we have employed a refined method compared to earlier works [11,12]. In addition to the commonly used two spin flipper arrangement we have cyclically permuted the polarizer

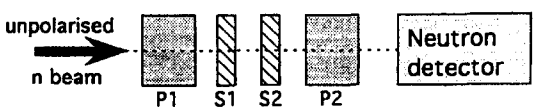

Fig. 5. Experimental arrangement for measuring p and s. Two spin flippers (S_1 and S_2) placed between the polarizer P_1 and the analyser P_2 were used. The unpolarized beam was chopped for this measurement to determine the neutron velocity by time of flight.

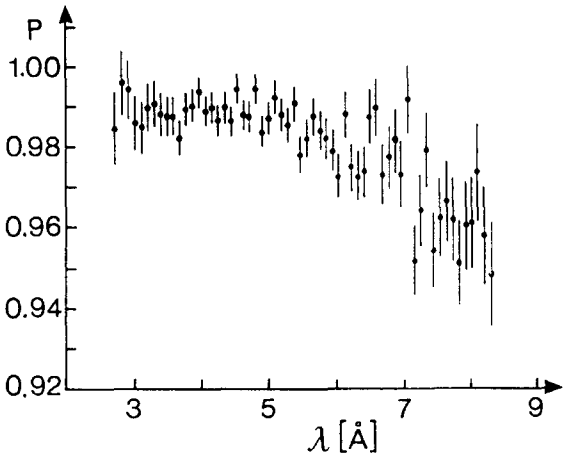

Fig. 6. The polarizing power of the polarizer used in the beta asymmetry measurement is plotted against the neutron wavelength.

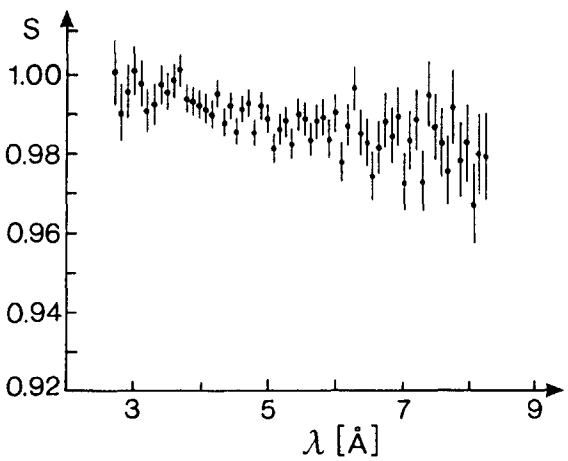

Fig. 7. Spin-flip efficiency plotted against the neutron wavelength for the spin flipper used in the beta asymmetry measurement.

and the analyser using three different bent super mirror polarizers. More details about the experimental set-up for measuring the neutron beam polarization are given in [7,8]. Fig. 6 shows an example for the polarizing power plotted against the neutron wavelength of polarizer P_1 and Fig. 7 shows the spin-flip efficiency plotted against the neutron wavelength for spin flipper S_1. For the asymmetry measurements the polarizer and spin flipper used gave the results of Figs. 6 and 7. To control the degree of polarization, the asymmetry measurements were interrupted and the beam catcher (Fig. 1) replaced by an analyser and neutron detector. For the mean value averaged over the neutron density distribution we obtained for the polarizer and spin flipper used in the final neutron beam line for the A measurement:

$$p = 0.981(3),$$

$$s = 0.990(2),$$
$$ps = 0.971 \pm 0.004. \tag{3}$$

The uncertainty includes the variation of the different polarization measurements. The polarization was measured with the whole neutron beam cross section and thus represents the beam averaged value. Since the spin flipper has less than 100% efficiency the degree of polarization in the decay volume is smaller with the spin flipper on. The electron spectra viewed by one detector for the case spin flipper off (W^+) and spin flipper on (W^-), respectively, are given by:

$$W^+ = W_0(E)\left(1 + \frac{v}{c} pA \cos\theta\right), \tag{4}$$
$$W^- = W_0(E)\left(1 + \frac{v}{c} pA \cos(\theta - 180°)(2s - 1)\right).$$

The asymmetry function results then in

$$\frac{W^+ - W^-}{W^+ + W^-} = A\frac{v}{c}\cos\theta ps / \left(1 + A\frac{v}{c}\cos\theta\, p(1-s)\right). \tag{5}$$

For the case of a high spin-flip efficiency the denominator in Eq. (5) is very close to one and only the product ps of the neutron beam must be known accurately. The measured spectra $N(E)$ are the spectra $W(E)$ convoluted with the detector response function (see Section 5.2). If $s = 1$ (perfect spin flipper) and $p = 1$ (perfect polarizer) Eq. (5) becomes identical to Eq. (2).

3.2. Measurement of the beta asymmetry

The measurements were carried out during two reactor cycles of 45 days at the PN7 beam of the ILL High Flux Reactor.

A typical run with neutrons lasted 18 hours without interruption. The drift chamber gas was renewed every two days.

Once per day the neutron beam was closed for calibration measurements. For the energy calibration sources with internal conversion electron lines (see Section 4.3) were moved into the drift chamber. A ^{204}Tl source was placed at one side of the drift chamber to measure electron tracks passing the whole chamber and thus measuring the efficiency of individual anode wires. Furthermore spectra without neutron beam were recorded once a day (^{6}LiF absorber after the spin flipper) to measure the background from the beam line, in particular from the polarizer.

4. Data reduction and analysis

4.1. Available data

The whole data were taken during three acquisition periods of one month each. The

Table 1
The number of events collected and kept for the analysis for the three acquisition periods.

	Events on tape	Events after cut
Period "1"	3.4×10^7	3.7×10^6
Period "2"	2.4×10^7	2.3×10^6
Period "3"	3.8×10^7	4.6×10^6
TOTAL	9.6×10^7	1.1×10^7

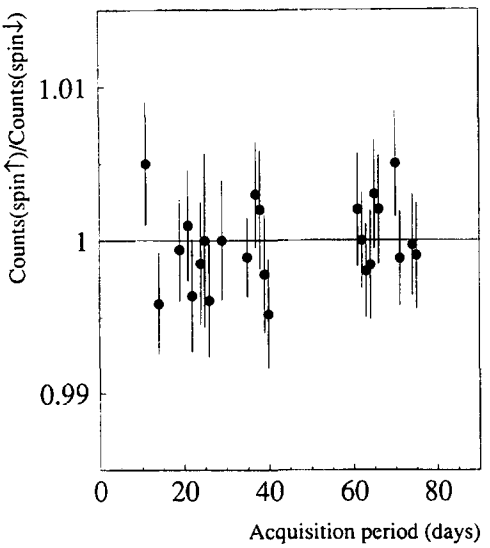

Fig. 8. The counting rate ratio of events collected with two different neutron spin directions is plotted against the acquisition time. A good stability has been observed over a 3 months acquisition period.

data were then compressed by selecting events satisfying the following conditions:
- the sum of both the signals collected at each PM at the end of the scintillator added off line agrees within 20 keV with the on-line recorded sum amplitude;
- the track, collected by the TPC anode and cathode wires, starts in the neutron beam area (central anode wires) and stops in the TPC border, touching at least 3 anode wires at the border and 1 cathode wire. This cut is mainly responsible for many rejections of events recorded on tape, since there was no hardware cut on the origin of the track.

The statistics before and after the software cuts are summarized in Table 1.

Several tests were performed in order to control the stability of the experimental conditions. The stability of the counting rate,the stability of the software cuts and the balance between two spin polarizations (Fig. 8) were controlled. About 95% of the data was taken to the further analysis.

4.2. Background analysis

The analysis of the β asymmetry is based on the careful subtraction of the

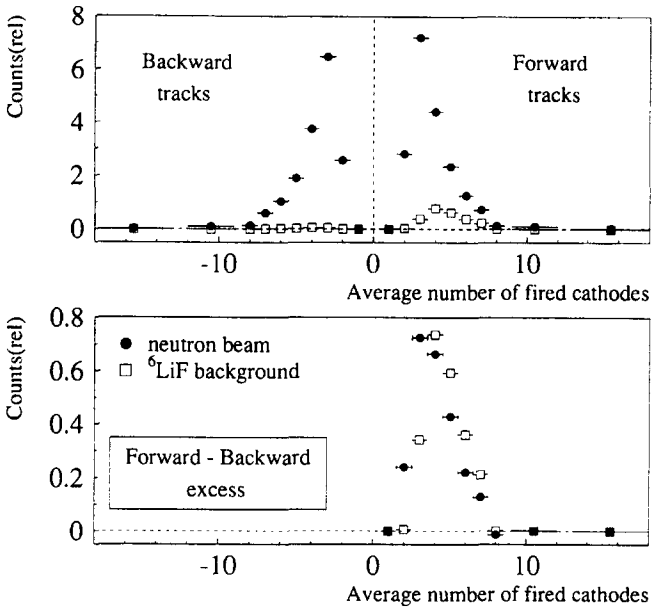

Fig. 9. The counting rate for electrons emitted in the forward and backward direction with respect to the neutron beam direction is plotted as a function of the number of fired cathodes. The forward–backward excess is the same for the neutron beam runs and for special runs where neutrons were completely absorbed by a ^{6}LiF absorber behind the spin flipper (see text).

background. The collected electrons were identified by their energy and their space origin. The determination of the background corrected signal is based on the combination of these two parameters. The main background was due to the Compton scattering of γ-rays by the detector gas. If a Compton electron was created in the region of the neutron beam it is selected like a true event.

The γ-rays produced by neutron capture in the polarizer gave the most important part of the background. These γ-rays were scattered by electrons of the atoms of the detector gas. The Compton electrons gave in turn a signal in the detector. To measure this component of the background, the neutrons were completely stopped by a 3 mm thick ^{6}LiF plate. This neutron absorber was located right after the spin flipper and did not modify in a perceptible manner the number of γ-rays reaching the detector.

On the average the counting rate with a ^{6}LiF absorber (called here "background ^{6}LiF") was less than 10% of that with the neutron beam. The trajectories of electrons in this background measurements are mainly pointed in the neutron beam direction as it is expected for Compton scattering. Let us define the forward–backward asymmetry for Compton electron trajectories as $a = (N_f - N_b)/(N_f + N_b)$ where N_f and N_b stand for forward and backward trajectories, respectively. For the background ^{6}LiF a value of $a = 0.8$ was observed when all cathodes were touched. A much smaller forward–backward asymmetry was present in the raw data with neutrons. After subtraction of this background this asymmetry vanished (Fig. 9).

The experimental β asymmetry defined as $(N^+ - N^-)/(N^+ + N^-)$ where N^+ (N^-)

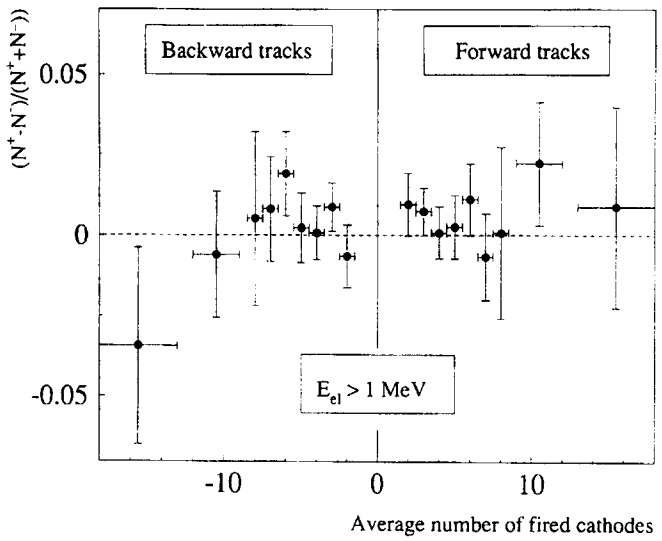

Fig. 10. Beta asymmetry for events of energy greater than 1 MeV plotted against the number of fired cathodes. It is compatible with zero.

stand for the spin flipper off–on was calculated for the background ^{6}LiF. The average value of the asymmetry $(4.6 \pm 4.0) \times 10^{-3}$ is compatible with zero. This averaged value does not depend on the number of fired cathodes.

The electron spectrum above 1 MeV consists only of background events. These background events are due to neutrons scattered by the gas and hence captured by surrounding materials and thus producing γ-rays. Neighbouring experiments and residual cosmic rays, which are not completely eliminated by the hardware cuts, participate to that component of the background. The β asymmetry for events above 1 MeV for all possible combinations of fired cathodes is compatible with a zero value $(2.9 \pm 5.3) \times 10^{-3}$. It does not show any asymmetry as a function of the number of fired cathodes (Fig. 10).

The hardware and software cuts select electrons originating from the neutron beam space in the xy (horizontal) plan (Fig. 2). The vertical position of the electron is given by the time of drift of the ionisation electrons toward the MWPC plane where the level discriminator on the scintillator pulse gives the $t_{\text{drift}} = 0$ signal and the level discriminators of the anodes below the neutron beam the stop signal. The distribution of the Δt_{drift} is shown in Fig. 11 for both spin states and both sides of the detector. It is seen that a part of electrons is not correlated with the position of the neutron beam and participates also to the background. Finally the background components discussed above were subtracted in the following way:

- The "neutron-free spectrum" (collected with the ^{6}Li absorber) was normalised to the same data acquisition time as the "neutron spectrum" and then subtracted. This procedure eliminates events originating from γ-rays accompanying the neutron beam and scattered in the detector gas by the Compton effect. This background component was about 5% of the signal from neutron decay.

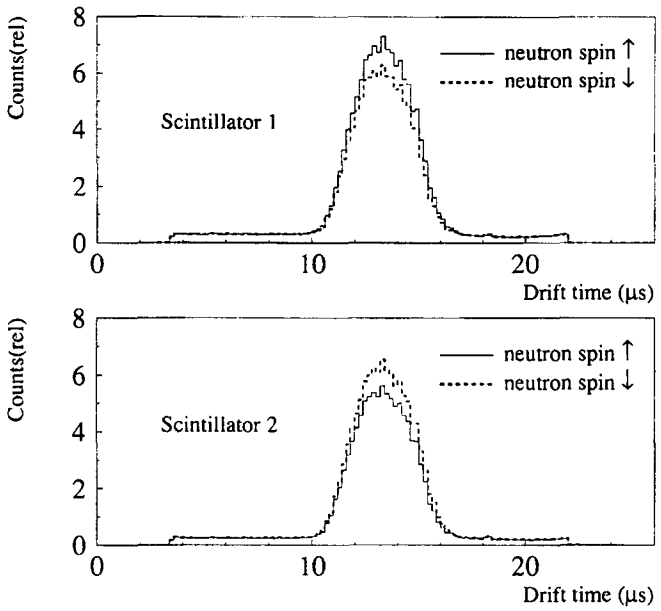

Fig. 11. Drift time spectra of decay electrons for both the neutron spin direction and for left and right detectors.

• The shape of the energy spectrum of the residual background was determined from the events originating from the outside of the neutron beam region (low and high drift time, Fig. 11). This background spectrum was normalised to the spectrum in the neutron beam region in the energy range above 1 MeV and then subtracted (background component about 3% of th the signal).

An uncertainty of 10% for the determination of the background level was estimated, i.e. 0.8% on the A coefficient measurement.

Fig. 14 illustrates the experimental energy spectra after background subtraction and the background component.

4.3. Energy calibration

The energy calibration of the data was performed with the internal conversion electron sources ^{139}Ce, ^{113}Sn and ^{207}Bi which were frequently moved into the drift chamber for the calibration measurements. The experimental lineshape (see Fig. 3) was parameterised by a Gaussian shape with a horizontal tail at the low-energy side. A low-energy cut-off at 90 keV was introduced corresponding to the electronic threshold and the low number of light quanta. Fig. 12 illustrates the lineshape used for the evaluation. The FWHM of the Gaussian shape was found as 220 keV at $E = 1000$ keV. Its energy dependence was chosen proportional to $\sqrt{E}$. The observed level of the horizontal tail was 6% of the line height at 364 keV and was chosen proportional to $1/\sqrt{E}$.

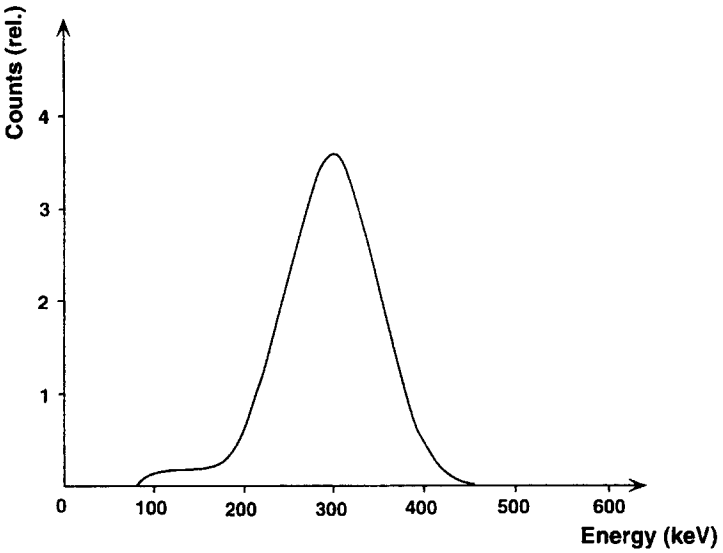

Fig. 12. Parametrisation of the experimental response of the plastic scintillator. A Gaussian shape with a horizontal tail and a cut-off at the low energy side was used. An example of the lineshape for an energy of 300 keV is shown.

For the calibration of energy versus channel number the position and intensity of K internal conversion lines were fit with the given lineshape. The position and intensity of outer internal conversion electrons were fixed relative to the K lines in the fit procedure. This energy calibration curve could be well described by a straight line. Then the calibration source was moved along the detector axis, the slope of the calibration curve changed by less than 5% and an average slope was used for the further evaluation.

4.4. Calculation of the averaged value of the cosine $\langle \cos\theta \rangle$ of the angle between the momentum of the decay electron and the neutron spin direction

As explained in Section 2 our TPC detector registered the trajectories of the decay electrons. The x coordinate along the neutron beam direction was given by the signal registered on 20 cathodes, but the spatial resolution along the x axis (2.5 cm) was not sufficient to allow a precise knowledge of the angle of the emitted electrons. For a given number of fired cathodes we used the Monte Carlo method to calculate the average value $\langle \cos\theta \rangle$. This average includes also the neutron beam profile and the scintillator size in z direction.

The angles φ and θ (Fig. 2) are randomly chosen, respectively, with a uniform and sine like distribution. The energy distribution of the electrons follows the allowed form of the β spectrum. The length of the neutron beam region from where the electrons originate is fixed by the chosen number of fired cathodes. The veto signals from the outermost cathodes (number 1,2 and 19,20) limit the useful length of the neutron beam

to 40 cm. The neutron density distribution and hence the distribution of the emitted electrons as a function of the z and y coordinates are close to Gaussian distributions and correspond to the measured profiles of the neutron beam. Along their paths, the electrons undergo multiple scattering from the detector gas (^{4}He(93%)–CO_2(7%)). The calculation was done by using a routine in which the electron track is calculated step-by-step through the gas medium. The electron is supposed to change its momentum direction as well as to lose some energy after each step.

The energy losses were calculated according to the Landau theory [13]. The mean value of the ionization potential is 58.1 eV for our gas mixture. A comparison between the calculated energy loss and data from pure ^{4}He shows a good agreement in the (100–780) keV energy range [14]. The standard deviation σ_{ms} due to multiple scattering for pure ^{4}He was calculated and measured in Ref. [15]. Corrected for the presence of the small amount of CO_2 in our gas mixture the value is $\sigma_{ms} \cong 0.94$ cm for electrons of 150 keV energy travelling through 10 cm of gas. The variations of σ_{ms} with the electron energy as well as the length of the electron path was taken into account event per event.

The lateral spreading of electrons moving through a gas under the action of uniform electric fields limits the spatial resolution of the detector. For our gas mixture (93% ^{4}He–7% CO_2) the lateral spreading leads to a distribution of the drifted electrons along x coordinate with a standard deviation σ_{drift}. The total lateral spreading is given by [16]:

$$\sigma_{tot} = \sqrt{\sigma_{drift}^2 + \sigma_{ns}^2},$$

$$\sigma_{drift} = \sqrt{2\frac{D}{\mu}\frac{z}{E}}. \tag{6}$$

D/μ is the ratio of the diffusion coefficient to the mobility of drifted electrons. E is the electric field and z the averaged distance over which the electrons are drifting. The D/μ values were obtained from Ref. [17]. The actual values for the used gas mixture were $E = 175$ V/cm, $z = 10$ cm and $\sigma_{drift} \cong 0.2$ cm.

In Table 2 we quote the averaged value of cos θ for both cases calculated with and without the influence of the multiple scattering.

The uncertainty due to some variations of the geometrical parameters was calculated for the following variations of the dimensions of the decay volume as well as for the variations of the dimensions and positions of the plastic scintillators:

beam: length: 40.0 ± 2.5 cm (one cathode width);

y and z neutron distribution $\Delta y = \Delta z = \pm 0.5$ cm at FWHM.

Table 2
The values of the $\langle \cos\theta \rangle$ obtained by simulations: (a) with multiple scattering and drifted electrons swarming and (b) without these two effects.

Cathodes number	1	2	3	4	5	6	7	all
(a)	0.957	0.926	0.844	0.747	0.654	0.575	0.512	0.850
(b)	0.959	0.926	0.844	0.742	0.647	0.563	0.497	0.847

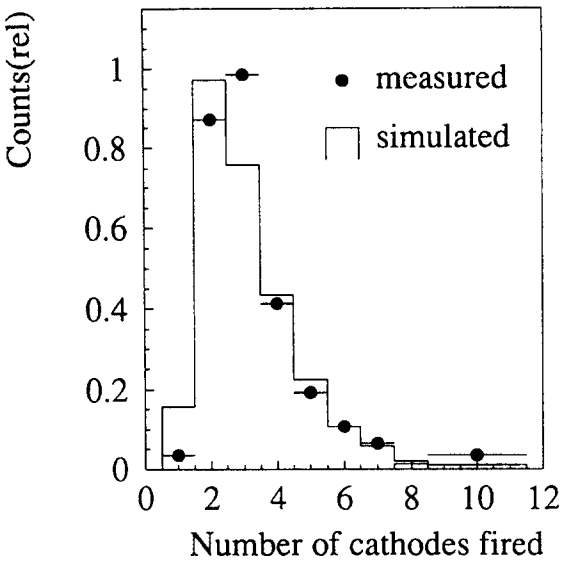

Fig. 13. The simulated distribution of the number of fired cathodes with value of 0.2 for a cross-talk coefficient is compared with the measured distribution.

scintillators: length: 43.0 ± 0.3 cm;
height: 14.6 ± 0.2 cm;
distance from beam centre 14.2 ± 0.2 cm.

The cross talk coefficient between two consecutive cathodes is determined in the following way: the β particle starts its trajectory in $y = z = 0$. The x coordinate is uniformly distributed over the cathode width; the θ' and φ angles are fixed so that the momentum of the β particle is directed along the y axis pointing towards the scintillator. The cross talk coefficient defined as the ratio of the number of two fired cathodes over the total number of events (1 + 2) cathode is found to be 0.20.

Fig. 13 shows the simulated distribution of the fired cathodes calculated with this "cross talk" coefficient; this distribution is compared to the measured one. The values of $\langle \cos \theta \rangle$ are given in Table 2. The uncertainty from the geometry was found to remain at a rather low level. It varies from 2×10^{-3} for 1 or 2 cathodes up to 2.5×10^{-2} for 7 cathodes. For the global average value of cos θ, when all the events were taken into account, we obtained:

$$\langle \cos \theta \rangle = 0.850 \pm 0.003. \tag{7}$$

This value is rather insensitive to the individual electron track measurement in the TPC but depends mainly on the fiducial volume, which is well defined by the vetoes from the outer cathodes. The uncertainty includes a variation of one cathode width for the length of the decay volume, which seems to be reasonable when the measured and calculated electron track distributions are considered (see Section 5).

5. Results

5.1. Experimental form of the beta spectrum

The experimentally recorded form of the beta spectrum from the free neutron decay differs from the allowed form because of the detector response. The main effects are backscattering of the decay electrons at the scintillator, the finite energy resolution of the detector, the energy cut-off of the electronics and the multiple scattering of the electrons in the drift chamber gas.

The resulting detector response was parametrised as described in Section 4.3. The allowed form was folded with this response function and then compared with the sum of the data for the two spin directions $N^+ + N^-$. The energy calibrated experimental pulse height spectra of the scintillator, $N(E)$, corresponds to the electron spectra $W(E)$, Eq. (4), convoluted with the detector response function. The measured end-point energy was too low by 25 keV and 34 keV for the left and right detector, respectively, compared to the known value of 782 keV. For the further evaluation the slope of the energy calibration was corrected accordingly. This difference may be due to the energy

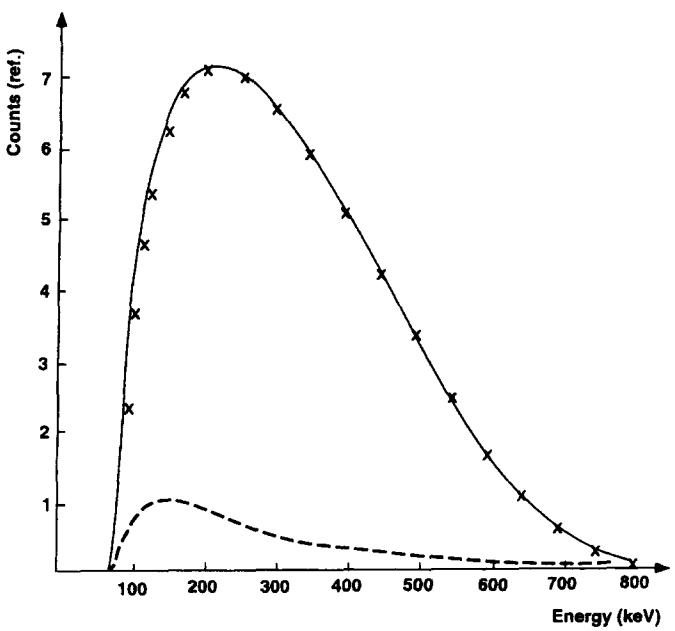

Fig. 14. The experimental beta spectrum $(N^+ + N^-)$ without selection of numbers of fired cathodes (continuous line) is compared to the allowed shape folded with the scintillator detector response (× sign). The level of the subtracted background is illustrated by the dashed line.

calibration procedure with internal conversion electrons following K-capture (Section 4.3). Secondary effects such as the simultaneous emission of Auger electrons and X-rays were not taken into account, but sum-up with a certain probability to the internal conversion lines.

In Fig. 14 the $N^+ + N^-$ spectrum without selection of number of cathodes but with the background subtracted as described in Section 4.2 is compared with the allowed shape folded with the detector response. A good agreement is observed. For the data subset of a selected number of cathodes fired the spectrum is deformed (see below). At lower energy the multiple scattering is stronger and hence it is less probable that the ionisation track remains straight.

In a second approach the influence of the drift chamber gas and plastic scintillator on the measured form of the beta spectrum was calculated. Data on electrons backscattered by bulk material in the 100–1000 keV range are not directly available for material like plastic scintillator ($(CH)_K$).

The coefficient of backscattering η and the energy losses for backscattered electrons from the plastic scintillator were deduced from data for heavier materials (Au, Ag, Cu, Al and LiF) found in [18–20]. The backscattering coefficient η is defined as the ratio of the backscattered electrons over the number of monoenergetic incident electrons. In the above quoted articles η has a nearly constant value as a function of the energy of the incident electron but depends strongly on the incidence angle of the incoming electron. The energy carried away by the backscattered electron can be, in a good approximation, fitted with a linear relation against the incident electron energy, and depends also on the angle of incidence.

From N electrons with an initial energy E_i, a fraction $\eta \cdot N$ is backscattered with a remaining energy E_{scatt}. Only the energy $(E_i - E_{scatt})$ is deposited in the plastic scintillator for those electrons and hence they are recorded as electrons of lower energy. The β spectrum is distorted and shifted towards lower energy values. The β spectrum was calculated from the theoretical allowed form taking into account the backscattering of the electrons by a scintillator, the influence of multiple scattering in the detector gas and the finite energy resolution of the scintillator. Fig. 15 compares the experimental spectrum and the calculated one for 7 cathodes fired. For this case the influence of backscattering is maximal. The allowed β spectrum is represented by a solid line. Fig. 16 shows the case of 2 cathodes fired. Owing to the η values which are extrapolated and not very accurate, the agreement between simulated and observed spectra is quite satisfactory.

5.2. *Experimental asymmetry and deduction of the asymmetry coefficient* A_0

For deducing the asymmetry coefficient from the measured data the experimental detector response function was taken into account. For this purpose the spectra W^+ and W^- in Eq. (4) were convoluted with the measured detector response function $R(E, E')$ parametrised as described in Section 4.3. For the correction function $C(E)$ the formal-

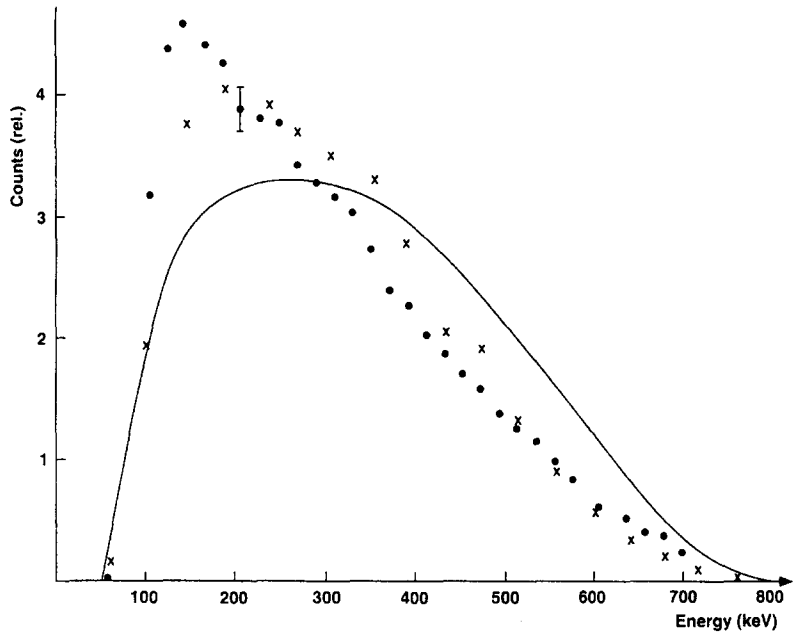

Fig. 15. The (x) sign represents the beta spectrum calculated from the theoretical shape taking into account the backscattering of the electrons by the plastic scintillator as well as the influence of the multiple scattering in the gas detector. For the case of 7 cathodes touched the figure compares this result with the experimental beta spectrum (solid circle). The continuous line represents the theoretical allowed shape convoluted with the measured detector response without selection of cathode number.

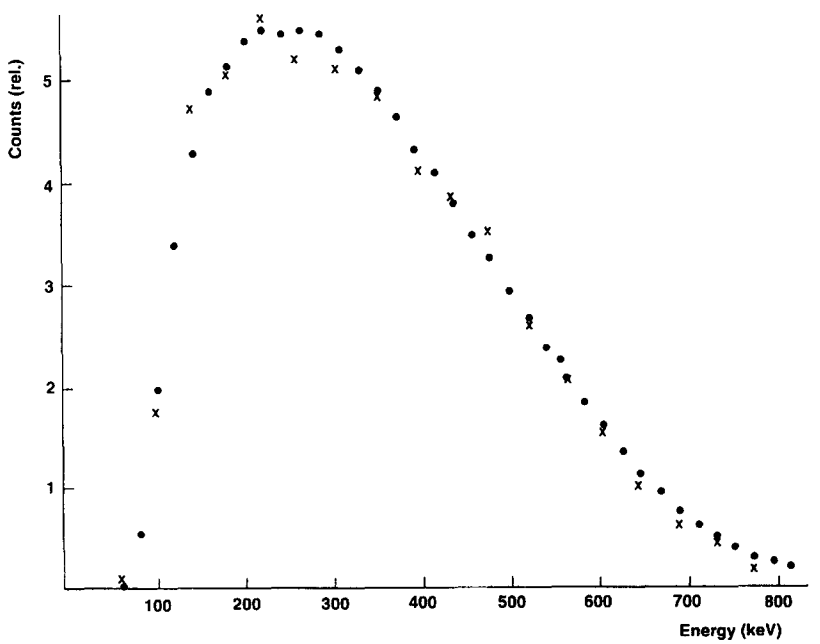

Fig. 16. The same as in 15 for (1 + 2) touched cathodes. The theoretical shape is not presented.

ism of Wilkinson [23] was used which takes into account recoil and weak magnetism. The modified asymmetry function Eq. (2) results then in

$$\frac{N^+ - N^-}{N^+ + N^-} = A's\frac{F(E)}{1 + A'(1-s)F(E)}, \tag{8}$$

$$F(E) = \frac{\int W_0(E')C(E')(v/c)R(E, E')\,dE'}{\int W_0(E')R(E, E')\,dE'}, \tag{9}$$

$A' = A_0\ p\cos\theta$, $C(E) = 1 - 0.0088 + 0.0141E + 0.0014/E$,

E is the total electron energy in units of the electron mass.

For the ideal response function $R(E, E') = \delta(E, E')$ the expression $F(E)$ becomes $C(E)v/c$ and Eq. (8) is identical to Eq. (5), with $A = A_0C(E)$.

Fig. 17 shows the experimental asymmetry as a function of the energy calibrated scintillator pulse height without restriction on the number of cathodes fired. The main dependence corresponds to the v/c term with small changes due to the detector response function. The solid curve shows the expected curve for a value of A' optimised by a least square fit. The χ^2/d.o.f. value of the fit was 0.7 and 1.1 for the left and right detector, respectively.

For the two detector sides the following values were found: $A'_1 = 0.0958 \pm 0.0010$ and $A'_2 = -0.0978 \pm 0.0010$ (sign change due to $\cos\theta$). This leads to an average value of $|A'| = 0.0967 \pm 0.0007$. The given uncertainties are statistical. The values from the right and left detector agree within the limits of the statistical accuracy proving the good symmetry of the experimental set-up. It should be noted that spurious effects, such as spin-flip related movements of the neutron beam or its polarisation profile, unequal measuring time for the two spin directions, neutron beam not perfectly centered, etc., do cancel in first order in the average over the two detectors.

The various systematic uncertainties on A_0 in the present experiment were already discussed above and in Table 3.

The total error is taken as the quadratic sum of the individual errors. This leads to the final result for A_0 (1σ error):

$$A_0 = \frac{A'}{p\langle\cos\theta\rangle} = -0.1160 \pm 0.0009\ (\text{stat.}) \pm 0.0012\ (\text{syst.})$$

$$= -0.1160 \pm 0.0015(1\sigma). \tag{10}$$

For a confidence level of 90% the statistical error has to be increased while the systematic error is already estimated conservatively. It leads to $A_0 = -0.1160 \pm 0.0019$ (90% C.L.).

This result is in good agreement with the experimental value of Ref. [4], but disagrees by two standard deviations with the PNPI value [3].

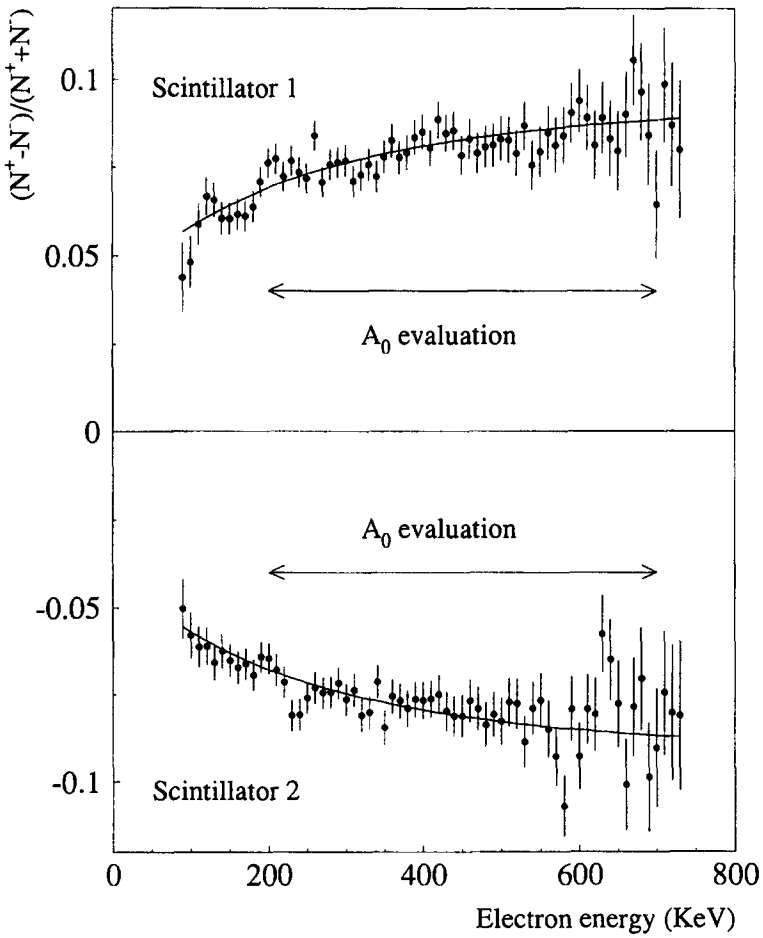

Fig. 17. The measured beta asymmetry between both spin states is presented for both scintillators. The continuous line represents the χ^2 fit to the counting asymmetry of the theoretical shape folded with the detector response function. The range used for the evaluation of A_0 is indicated (200–700 keV).

Table 3

background substraction	0.8%
determination of p	0.3%
determination of s	0.2%
energy calibration	0.4%
$\langle \cos\theta \rangle$	0.4%

5.3. Different view of the asymmetry uncertainties

Let us now analyse the data in terms of the experimental ratio R, which leads directly to the average A value of the left and right detector:

$$R = \frac{N_R^+ N_L^-}{N_R^- N_L^+}. \tag{11}$$

The counting rate for the right detector and the neutron spin directions can be written as:

$$N_R^+ = Y\Omega_r \varepsilon_{rc} \varepsilon_{rs}(1 + Ak_p),$$
$$N_R^- = Y\Omega_r \varepsilon_{rc} \varepsilon_{rs}(1 - Akp(2s - 1)). \tag{12}$$

Y is the normalisation to the neutron beam intensity, Ω_r is the solid angle seen by the decay volume for the right detector. The ε_{rc} and ε_{rs} are the detection efficiencies for the drift chamber and the scintillator, respectively. A similar expression can be written for the left detector. The quantity k denotes the product $\langle v/c \rangle \langle \cos\theta \rangle$. The experimental ratio does not depend on Y. This ratio does also not depend on Ω's and ε's as far as these parameters do not vary with the neutron spin direction. For s close to 1 and hence $2s - 1 = s^2$ the experimental ratio is then:

$$R = \left(\frac{1 + Akps}{1 - Akps}\right)^2 \quad \text{and} \quad A = \frac{1}{kps}\frac{\sqrt{R} - 1}{\sqrt{R} + 1}, \tag{13}$$

$$\frac{\Delta A}{A} = \sqrt{\left(\frac{\sqrt{R}}{R-1}\frac{\Delta R}{R}\right)^2 + \left(\frac{\Delta k}{k}\right)^2 + \left(\frac{\Delta p}{p}\right)^2 + \left(\frac{\Delta s}{s}\right)^2}. \tag{14}$$

We actually have to analyse the possible error in the experimental ratio R, the error in ps as well as the errors in the calculated value of the geometrical coefficient k. Let us start with the possible errors on R. The previous calculation has shown that R is not influenced by fluctuation in the beam intensity, detection efficiency and changes in the detector solid angle. N_R^+ and N_L^+ are measured within the same time interval Δt, N_R^- and N_L^- during $\Delta t'$; in the formula Δt and $\Delta t'$ cancel exactly, so the inequality in counting time cannot account for any error. The uncertainties for k, p and s enter in ΔA as in Section 5.2.

The decay probability is written as:

$$W(E) \propto 1 + b\frac{m}{E_e} + a\frac{P_e P_\nu}{E_e E_\nu} + \sigma_n \cdot \left(A\frac{P_e}{E_e} + B\frac{P_\nu}{E_\nu} + D\frac{P_e \times P_\nu}{E_e E_\nu}\right) \tag{15}$$

where P_e, P_ν, E_e and E_ν are the leptons momenta and total energies; σ_n is the neutron spin vector. The a, B and D coefficients have clearly no influence since the recoil proton and hence the antineutrino is not detected. The only coefficient which could interfere in our measurement is the term of Fierz (bm/E_e); b is smaller than 6×10^{-3} [21], leading to $(bm/E_e) \leqslant 3 \times 10^{-3}$. The experimental ratio becomes:

$$R' = \left(\frac{1 + Akps + bm/E_e}{1 - Akps + bm/E_e}\right)^2 \quad \text{or} \quad R' = R\left(\frac{1+Z}{1+Z'}\right)^2, \tag{16}$$

where

$$Z = \frac{bm/E_e}{1 + Akps} \quad \text{and} \quad Z' = \frac{bm/E_e}{1 - Akps}$$

$$k = 0.075, \qquad ps = 0.971, \qquad R' = 0.999R,$$

so that the systematic error due to the Fierz term is smaller than 0.001 on R which leads to $\Delta A/A \leqslant 0.003$.

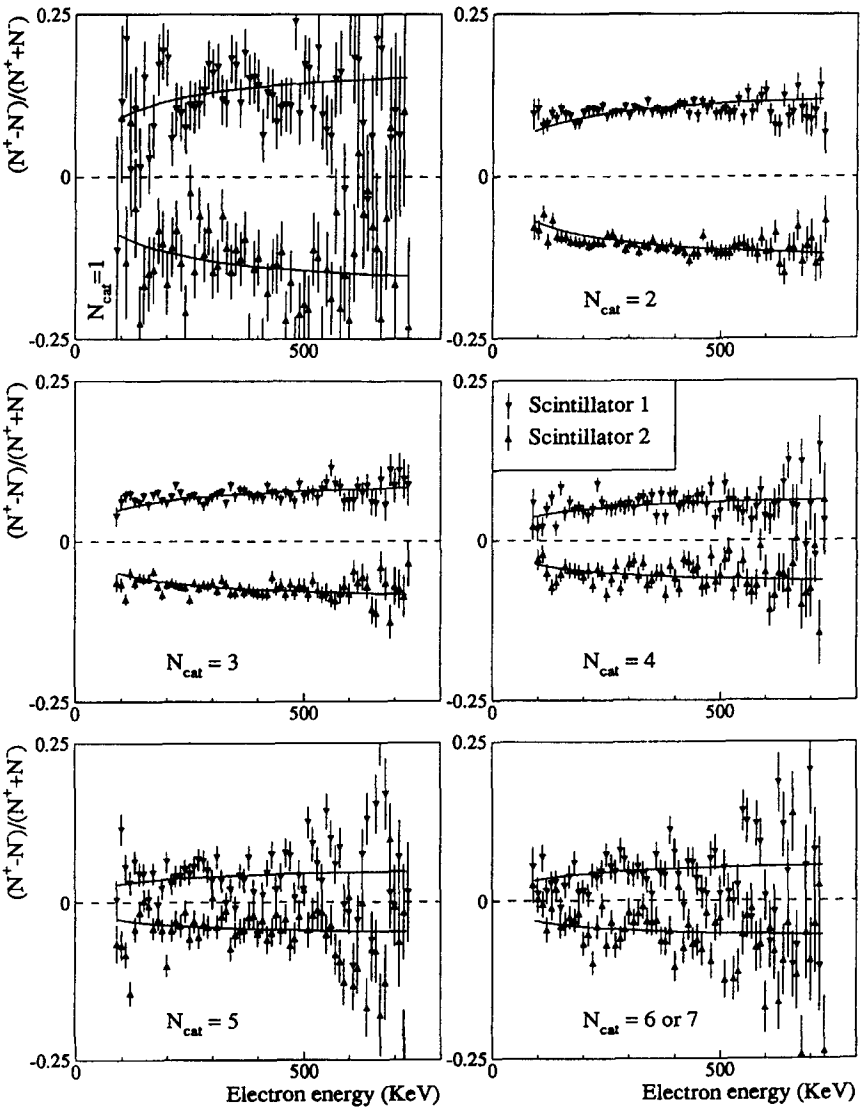

Fig. 18. Same as Fig. 17, but presented separately for each number of cathodes fired. The (χ^2 fits) (performed between 200–700 keV) for each data subsample is presented.

5.4. Angular distribution of the asymmetry

Large values for the angle θ between the decay electron emission and the neutron spin direction (y direction) were observable in our experiment only along the x components. The track length in the x direction was given by the number of cathodes fired, where a low number of cathodes fired corresponded to a small angle θ. The observable size of a z component was limited by the scintillator height and allowed only a maximum angle θ in the (y, z) plane of about 30°.

In a separate data evaluation, events were selected by a number of cathodes fired and analysed individually. In a first step the form of the sum spectra ($N^+ + N^-$) for those data was compared with the spectral shape of the data without cathode selection and with the simulations (Figs. 14–16). A significant distortion was observed compared to the global spectra. Qualitatively the effect could be due to a loss in low-energy events for a low number of cathodes and a gain in low-energy events for a high number of cathodes (see Figs. 15 and 16). The track of low-energy electrons is less straight and the specific gas ionisation is stronger; hence it is unlikely to trigger only a low number of cathodes. These for low cathode numbers lost events are then recovered in cuts with a higher number of cathodes. The simulation for different numbers of cathodes fired underestimates this effect (Figs. 15, 16) and a quantitative shape simulation was not

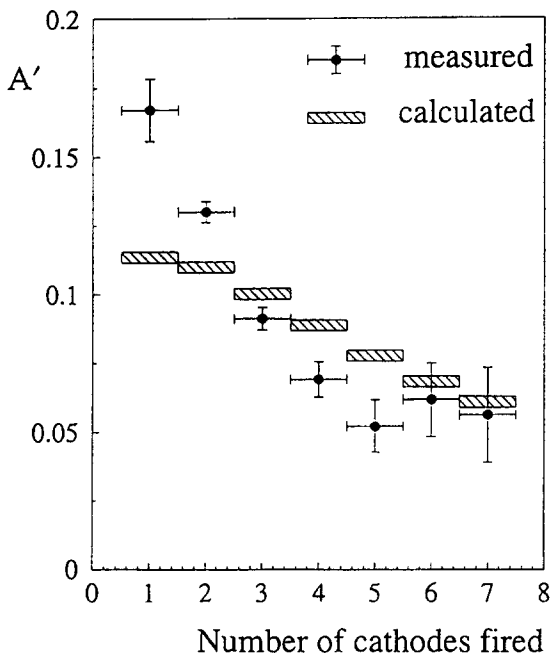

Fig. 19. The measured asymmetry A' (points) is represented as a function of the number of fired cathodes. The hatched areas indicate the values calculated from the asymmetry measured without selection of numbers of fired cathodes and corrected for the expected cos θ dependence, and electron track simulation (Section 4.4). The observed distribution deviates significantly from the cos θ based expectation.

achieved. For the further treatment of the selected data an energy-dependent efficiency correction term of an empirical form $(1.-q/E)$ was added, with the free parameter q and the electron energy E. For different number of cathodes this parameter was positive or negative and allowed a good description of the observed spectral shape.

In the next step the asymmetry A_i for each number i of cathodes was evaluated by a least square fit (Fig. 18). The fit results of the combined data from the left and right scintillator (formalism of Section 5.3) are plotted in Fig. 17. The given errors include the statistical error, the error in energy calibration and background subtraction. For comparison the expected distribution for the cos θ law is shown (Fig. 19). The corresponding values are calculated with the A_0 result from the global evaluation and the track simulation explained in Section 4.4.

6. Final result and conclusions

From our experiment we adopted the asymmetry parameter $A_0 = -0.1160(15)$ obtained from the evaluation of the data without selection of the number of cathodes and with the consistent results from the two scintillators (Section 5.2). In this evaluation the detection volume was well defined by the veto signals from the outer cathodes and the size of the scintillators. As discussed in Section 4.4 the $\langle \cos\theta \rangle$ value of 0.850(3) as the average over the decay volume is quite insensitive to the details of the electron tracks and especially to multiple scattering effects.

Within the standard model the beta asymmetry is linked to the ratio g_A/g_V in the following way:

$$\lambda = |\lambda| e^{i\phi} = g_A/g_V, \tag{17}$$

$$A_0 = -2\frac{\lambda^2 - |\lambda| \cos\phi}{1+3\lambda^2}. \tag{18}$$

The measurement of the D coefficient (Time Reversal Invariance) gives $\theta = 180.14 \pm 0.22°$ (22), so that

$$A_0 = -2\frac{\lambda^2+\lambda}{1+3\lambda^2}, \tag{19}$$

$$\lambda = -\frac{1+\sqrt{1-A_0(3A_0+2)}}{3A_0+2}, \tag{20}$$

$$\frac{\Delta\lambda}{\lambda} = 0.25\left(\frac{\Delta A_0}{A_0}\right), \tag{21}$$

with our results $A_0 = -0.1160$ (15) we obtain

$$\lambda = -1.266(4). \tag{22}$$

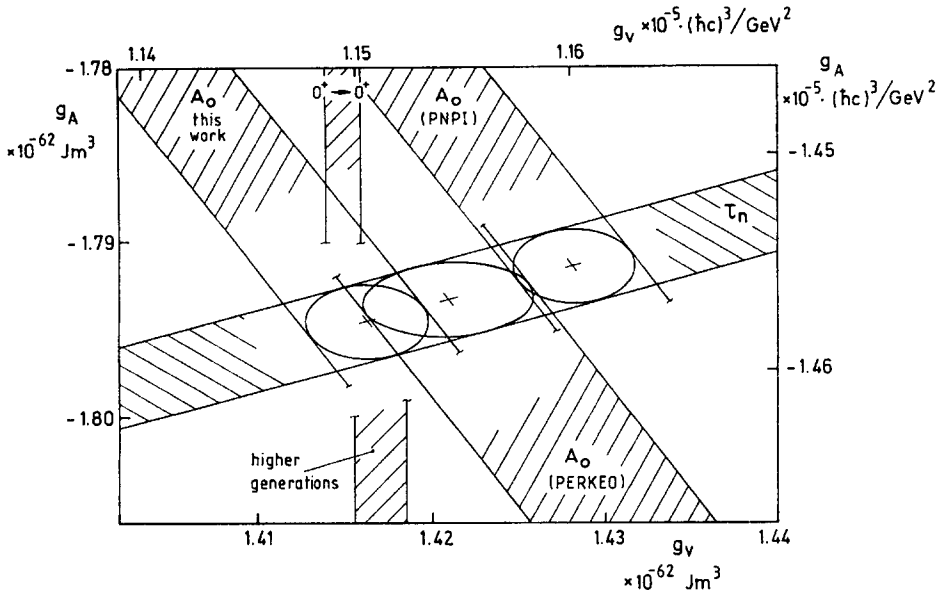

Fig. 20. Comparison of experimental weak interaction coupling constants in units of J·m^3 and $(\hbar c)^3/\mathrm{GeV}^2$. The ellipse shows the 1σ uncertainty contours for g_A/g_V deduced from neutron decay data with different experimental results for A_0, from left this work, PERKEO [4], PNPI [3]. The g_V values from ft $(0^+ \to 0^+)$ and from the muon decay (higher generation) are also given.

Using the present mean value for the neutron lifetime $\tau_n = 887.4\ (1.7)$ s the vector coupling constant g_V and the axial vector coupling constant g_A could be deduced from the neutron beta decay alone yielding

$$g_V = 1.4172(34) \times 10^{-62}\ \mathrm{J \cdot m^3} = 1.1511(28) \times 10^{-5} \frac{(\hbar c)^3}{\mathrm{GeV}^2},$$

$$g_A = -1.7944(20) \times 10^{-62}\ \mathrm{J \cdot m^3} = -1.4575(17) \times 10^{-5} \frac{(\hbar c)^3}{\mathrm{GeV}^2}. \qquad (23)$$

The two last precise measurements of A_0 are:

$$A_0 = -0.1146 \pm 0.0019 \quad (\text{Ref. [4]}), \qquad \lambda = -1.262 \pm 0.005,$$
$$A_0 = -0.1116 \pm 0.0014 \quad (\text{Ref. [3]}), \qquad \lambda = -1.2544 \pm 0.0036. \qquad (24)$$

Our result agrees within the uncertainties with that of Ref. [4]. In Ref. [4] the β asymmetry was obtained by measuring only the decay electrons. In Ref. [3] the recoil proton was detected in coincidence with the emitted electron. A_0 was evaluated for the similar energy range in Refs. [3,4] and for the result presented in this paper. The corresponding evaluations for g_V and g_A are shown in Fig. 20 and are compared with g_V from $ft(0^+ \to 0^+)$ and muon decay (see Ref. [1]). Moreover, we have evaluated seperately the asymmetry for selected ranges in the electron emission angle θ relative to the neutron spin. The agreement with a simulation based on the cos θ law, the track simulation including multiple scattering and the global value of A_0 was rather poor

(Fig. 19). Background corrections, time jitter in the TPC, not perfect description of spectral shape or track simulations should not affect the asymmetry values in first order and can hardly explain the observed differences. Furthermore it is generally assumed that the cos θ law is valid, since it emerges naturally from the angular momentum coupling in the neutron decay – although this distribution has not been measured previously. Thus this detail in our evaluation remains unexplained.

The global evaluation of A_0 was done seperately and is not based on the individual tracks, but essentially on the limitation of the observed decay volume and the cos θ law. Thus it uses similar information than earlier measurements of the asymmetry parameter and is adopted in the present work.

In a new beta asymmetry experiment foreseen we should be able to improve the technics of measurement mainly by passing the neutron beam through vacuum or low-pressure helium and thus suppressing the main component of the background due to Compton scattering of γ-rays from the gas detector. A much better spatial resolution on the cathodes (x coordinates) is easily attainable so that we should get a more refined determination of the angle θ. A new cold neutron beam is about to be installed at the Laue–Langevin reactor. The higher expected cold polarized neutron flux will be of great help for improving the counting rate in the experiment.

Acknowledgements

We are indebted to the technical staff of the Laue–Langevin Institute and of the Institut des Sciences Nucléaires de Grenoble, especially to B. Guerre-Chaley and R. Bosson for their help in the construction and maintenance of the electronics and D. Robinson and J. Joubineau for mechanics. We acknowledge the Laboratoire de Physique des Particules d'Annecy which supplied us with numerous electronic devices. We also wish to thank Ph. Ledebt for his invaluable assistance with the hardware and software of the data acquisition system. We would like also to thank the students K. Jacob and J. Lamas-Valverde for computing Monte Carlo simulation for the experiment.

References

[1] D. Dubbers, W. Mampe and J. Dorner, Europhys. Lett. 11 (1990) 195;
K. Schreckenbach and W. Mampe, J. Phys. G 18 (1992) 1.

[2] V.A. Wickers, T.R. Hageman, J. van Klinken, H.W. Wilschut and D. Atkinson, Phys. Rev. Lett. 58 (1987) 1821;
A.S. Carnoy, J. Deutsch, R. Prieels, N. Severijns and P.A. Quin, J. Phys. G 18 (1992) 823;
Yu.V. Gaponov, N.B. Shulgina and P.E. Spivak, Phys. Lett. B 353 (1991) 283;
N.B. Shul'gina, Phys. Rev. Lett. 73 (1994) 2658.

[3] B.G. Erozolimskii, I.A. Kuznetsov, I.V. Stepanenko, I.A. Kuida and Yu.A. Mostovoi; Phys. Lett. B 263 (1991) 33; Sov. J. Nucl. Phys. 52 (1990) 999.

[4] P. Bopp, D. Dubbers, L. Hornig, E. Klemt, J. Last, H. Schütze, S.J. Freedman and O. Schärpf, Phys. Rev. Lett. 56 (1986) 919;

E. Klemt, P. Bopp, L. Hornig, J. Last, S.J. Freedman, D. Dubbers and O. Schärpf, Z. Phys. C 37 (1988) 179.
[5] K. Schreckenbach, P. Liaud, R. Kossakowski, H. Nastoll, A. Bussière and J.P. Guillaud, Phys. Lett. B 349 (1995) 427.
[6] O. Schärpf and N. Stuesser, Nucl. Instr. Meth. A 284 (1989) 208;
W.G. Williams, Polarised neutrons (Oxford Science, Oxford, 1988) p. 131.
[7] H. Nastoll, Diplomarbeit Mesure de la polarisation d'un faisceau de neutrons froids, Université de Karlsruhe/ILL 1991.
[8] H. Nastoll, K. Schreckenbach, C. Baglin, A. Bussière, J.P. Guillaud, R. Kossakowski and P. Liaud, Nucl. Instr. Meth. A 306 (1991) 65.
[9] R. Kossakowski, P. Grivot, P. Liaud, K. Schreckenbach and G. Azuelos, Nucl. Phys. A 503 (1989) 473; P. Grivot, R. Kossakowski, P. Liaud, K. Schreckenbach, G. Azuelos, A. Bussière and P. de Saintignon, Nucl. Instr. Meth. B 34 (1988) 127.
[10] A. Bussière, J. Chauvin, P. Grivot, R. Kossakowski, P. Liaud, P. de Saintignon and K. Schreckenbach, J. Phys. E 21 (1988) 1183.
[11] H. Kendrick, S.A. Werner and A. Arrot, Nucl. Instr. Meth. 68 (1969) 50.
[12] W. Vorbrugg, Nucl. Instr. Meth. 145 (1977) 311.
[13] L. Landau, J. Phys. (USSR) 8 (1944) 201.
[14] Pages et al., Nucl. Data 4 (1972) 1.
[15] R.C. Smith and B.W. Schumacher, Nucl. Inst. Meth. 118 (1974) 73;
J.F. Lawry and B.W. Schumacher, Nucl. Inst. Meth. 130 (1975) 577.
[16] G. Schültz and J. Gresser, Nucl. Inst. Meth. 151 (1978) 413.
[17] R.W. Wanen and J.H. Parker Jr., Phys. Rev. 128 (1962) 2661.
[18] A.J. Antolak and W. Williamson Jr., J. Appl. Phys. 58 (1985) 526.
[19] J. Kalef-ezra, Y.S. Horowitz and J.M. Mack, Nucl. Instr. Meth. 195 (1982) 587.
[20] G. Soum, A. Mousselli, F. Arnal and P. Verdier, Revue Phys. Appl. 22 (1987) 1189.
[21] Hardy and Towner, Nucl. Phys. A 254 (1975) 221.
[22] R.I. Steinberg, P. Liaud, B. Vignon and V.W. Hughes, Phys. Rev. D 13 (1976) 2469.
[23] D.H. Wilkinson, Nucl. Phys. A 377 (1982) 474.